RESEARCH ARTICLE

Check for updates

Tailoring metal sites of FeCo-MOF nanozymes for significantly enhanced peroxidase-like activity†

Xiqing Cheng, [a,b] Yameng Xie, [b] Guang Li, [b] Zhiping Zheng[b] and Qin Kuang (ID) *[b]

As a type of novel artificial enzyme, metal–organic frameworks (MOFs) have attracted great research interest due to their unique inorganic–organic hybrid structure, which can be designed to exhibit different enzyme mimicking activities *via* finely tuning metal nodes and coordination environments. In this work, a mixed metal–organic framework (FeCo-MOF-H_2) with excellent peroxidase-like catalytic activity was successfully prepared *via* low-temperature heat treatment in Ar/H_2 on Co-doped Fe-based MOFs. Based on the results of a variety of spectroscopic characterization processes, it was found that the electronic structure, chemical state and coordination environment of Fe sites in Fe-based MOFs were modulated by Co doping and low-temperature heat treatment, which synergistically contribute to selective H_2O_2 adsorption (HOOH$_{ad}$), catalysis and fast electron transfer at those accessible metal sites for producing hydroxyl radicals (•OH). Strikingly, *in situ* attenuated total reflection Fourier transform infrared (ATR-FTIR) spectrometry and steady-state kinetic studies showed that FeCo-MOF-H_2 has higher affinity to H_2O_2 (a smaller K_m value of 0.06 mM) even when compared with natural HRP as well as reported Fe-based and Co-based nanozymes. The catalytic activity of FeCo-MOF-H_2 was about 10.6 and 2.9 times compared to the pristine Co-MOF and Fe-MOF, respectively. Owing to their excellent peroxidase-like catalytic activity, the FeCo-MOF-H_2 nanozymes showed great application potential in the detection of H_2O_2 and glutathione, and the limit of detection and linear range are superior to those of most of the Fe-based and Co-based nanozymes reported so far. Our work provides a meaningful guidance for gaining insight into the structure–activity relationship of multivariate MOF-based nanozymes.

1. Introduction

Nanozymes, a class of nanomaterials with the characteristics of enzyme-mimicking activity, have received enormous attention in recent years due to their flexible and tunable activity and high stability.[1–4] However, the catalytic activity and selectivity of nanozymes are still not comparable to those of natural enzymes. As we know, the active center of metalloenzymes (*e.g.*, horseradish peroxidase, HRP) contains metal ions acting as catalytic groups or activators, as well as enzyme proteins that recognize substrates.[5–8] In this regard, the composition and structure of nanozymes are far different from those of the active centers of natural enzymes.[8–12] Meanwhile, the catalytic mechanism of nanozymes is still unclear to date, which also

seriously hinders the rational construction of nanozymes. Therefore, it is necessary to systematically reveal the catalytic process of nanozymes and to gain insight into the structure–activity relationship of nanozymes.

Among numerous enzyme-mimicking nanomaterials, metal–organic frameworks (MOFs) composed of metal nodes and organic ligands allow for flexible tuning of metal nodes and their coordination structure, and thus they are regarded as an ideal platform to identify the structure–activity relationships of nanozymes.[13–18] Although impressive progress has been made in improving the performance of MOF-based nanozymes,[19–22] most simple MOFs with single metal nodes and ligands hardly mimic the complex spatial structure and coordination environment of the active centers of natural enzymes. Clearly, it is difficult for pristine MOF-based nanozymes with a single-metal node and fully coordinated environment to achieve the same excellent performance as natural enzymes. Thus, mixed MOF-based nanozymes with dual-metal or multiple active sites are highly desired.[23–25] Recently, Wang and co-workers designed and prepared Mn/Fe-MIL(53) with Mn and Fe dual metal active sites, in which the doping of Mn enables highly sensitive and selective colorimetric detection of organophosphorus pesticides.[26] Very recently, we reported

[a]School of Chemical and Environmental Engineering, Shanghai Institute of Technology, 100 Haiquan Road, Shanghai 201418, China
[b]State Key Laboratory of Physical Chemistry of Solid Surfaces & Department of Chemistry, College of Chemistry and Chemical Engineering, Xiamen University, Xiamen 361005, Fujian, P. R. China. E-mail: qkuang@xmu.edu.cn;
Fax: (+) 86-592-2183047

This journal is © the Partner Organisations 2023

Inorg. Chem. Front., 2023, **10**, 2335–2343 | **2335**

mixed-valence Ni$_{4.8}$Fe-MOF peroxidase-like nanozymes with highly sensitive and selective sensing, in which Ni^{II} and mixed-valence Fe^{II}/Fe^{III} metal nodes within 1D sub-nanochannels synergistically enhanced the affinity for H$_2$O$_2$ and catalytic activity.[27] Remarkably, coordinatively unsaturated metal sites or open metal sites in MOFs can serve as substrate adsorption sites, which can selectively enrich substrates at or near catalytic sites.[18] Nevertheless, ways to construct accessible open sites conducive to substrate adsorption for MOF-based nanozymes have rarely been explored. Furthermore, the substrate adsorption process on MOF-based nanozymes has not been tracked *in situ*.

In this study, we proposed a low-temperature heat treatment strategy to fabricate mixed metal FeCo-MOF peroxidase-like nanozymes (named FeCo-MOF-H$_2$), and analyzed in detail the electronic structure and coordination environment of metal sites in nanozymes. In particular, the selective adsorption and catalytic mechanisms of the as-synthesized FeCo-MOF-H$_2$ peroxidase-like nanozymes were systematically studied by *in situ* attenuated total reflection Fourier transform infrared (ATR-FTIR) spectrometry, X-ray photoelectron spectroscopy (XPS), and electron spin-resonance spectroscopy (ESR). To our delight, this FeCo-MOF-H$_2$ as a peroxidase-like nanozyme sensing platform exhibited excellent performance in detecting H$_2$O$_2$ and glutathione (GSH).

2. Experimental section

2.1. Reagents and chemicals

Iron(III) chloride hexahydrate (FeCl$_3$·6H$_2$O), cobalt(II) nitrate hexahydrate (Co(NO$_3$)$_2$·6H$_2$O), *N,N*-dimethylacetamide (DMA), sodium acetate (NaAc), acetic acid (HAc), and hydrogen peroxide (H$_2$O$_2$, 30%) were obtained from Sinopharm Chemical Reagent Co. Ltd (Shanghai, China). Terephthalic acid (H$_2$BDC), 3,3′,5,5′-tetramethylbenzidine (TMB), and L-glutathione (reduced, GSH) were obtained from Alfa Aesar. 5,5′-Dimethyl-1-pyrroline-oxide (DMPO) was obtained from Energy Chemical (Shanghai, China). All the above chemical reagents were used directly without any treatment, and all experiments were conducted in ultrapure water.

2.2. Instruments

Scanning electron microscopy (SEM) images were recorded by field emission scanning electron microscopy (FE-SEM, HITACHI-S4800, Japan). The transmission electron microscopy (TEM) and energy dispersive spectroscopy (EDS) element mapping of nanozymes were performed on a transmission electron microscope (TEM, Tecnai F30, USA, 300 kV). Powder X-ray diffraction (XRD) patterns were obtained on an UltimaIV using Cu Kα radiation at λ = 1.5418 Å, 40 kV, and 40 mA. X-ray photoelectron spectroscopy (XPS) data were collected on a Thermo Scientific ESCALAB Xi+ spectrometer. Thermogravimetric analysis (TGA) was conducted on a TA instrument (SDT Q600, USA) under N$_2$ flow. The Fourier transform infrared (FT-IR) spectra were obtained by using a Thermo

Nicolet 380 spectrophotometer. *In situ* attenuated total reflection Fourier transform infrared (ATR-FTIR) spectra were recorded on a Thermo Nicolet Nexus 870 spectrophotometer. Electron spin resonance (ESR) spectra of hydroxyl radical (˙OH) signals were obtained by using a Bruker X-band A200. The steady-state kinetic experiments were performed on a UV-2550 spectrophotometer (Shimadzu, Japan) and other colorimetric experiments were measured using a multimode microplate reader (Tecan, Infinite M200).

2.3. Synthesis of nanozymes

Mixed-valence FeCo-MOF nanozymes were prepared through a two-step process. First, H$_2$BDC (0.083 g), FeCl$_3$·6H$_2$O (0.135 g, 0.5 mmol), and Co(NO$_3$)$_2$·6H$_2$O (0.5243 g, 1.8 mmol) were ultrasonically dissolved in DMA (12 mL) and the resulting solution was heated in a 20 mL Teflon-lined stainless steel autoclave at 150 °C for 3 h. After cooling to room temperature, the prepared FeCo-MOF was washed several times with ethanol and water and then freeze-dried. Afterwards, the obtained FeCo-MOF was placed in a tube furnace for further heat-treatment at 200 °C for 1 h under a H$_2$/Ar (5:95) atmosphere. Here, the resulting product was named FeCo-MOF-H$_2$. The Fe-MOF and Co-MOF were prepared in a similar route to FeCo-MOF except that Co(NO$_3$)$_2$·6H$_2$O or FeCl$_3$·6H$_2$O was not added.

2.4. Enzyme-mimicking activity assay

The enzyme-mimicking activities of the samples were assessed in 96-well plates by using TMB and H$_2$O$_2$ as substrates. To assess the peroxidase-like activity of the as-prepared samples, 8 μL of TMB (20 mM) was first added into 185 μL of sodium acetate buffer (0.2 M, pH = 3.6). Then, 2 μL of H$_2$O$_2$ (100 mM) and 5 μL of 1 mg mL^{-1} MOF samples (*i.e.*, FeCo-MOF-H$_2$, FeCo-MOF, Fe-MOF, or Co-MOF) were sequentially added into the above mixture. After a 3-minute incubation, UV-Vis absorption spectra of the mixture were recorded with a multimode microplate reader. The oxidase-like activity of the samples was evaluated by a similar experimental procedure to the peroxidase-like activity, except that no H$_2$O$_2$ substrate was added.

2.5. Steady-state kinetic study

The steady-state kinetics of FeCo-MOF-H$_2$ nanozymes was measured on a UV-vis spectrophotometer at room temperature. The experiments were carried out at a fixed concentration of H$_2$O$_2$ or TMB, while adjusting the concentration of the other reagent. For example, 10 μL of TMB (20 mM), 25 μL of FeCo-MOF-H$_2$ (1 mg mL^{-1}) and 40 μL of various concentrations of H$_2$O$_2$ were added into 935 μL of sodium acetate buffer (0.2 M, pH = 3.6). The absorbance of the resulting solution at 652 nm was then quickly measured within 1 minute. Finally, a Michaelis–Menten curve was fitted with the concentration of H$_2$O$_2$ and the corresponding initial velocity was calculated from the absorbance changes within 1 minute. For the TMB substrate, the kinetics measurements were similar to those for H$_2$O$_2$, expect that the concentration of TMB was changed.

2336 | *Inorg. Chem. Front.*, 2023, **10**, 2335–2343

This journal is © the Partner Organisations 2023

2.6. *In situ* ATR-FTIR spectroscopy

To study the behavior of the substrate H_2O_2 in the reaction, 10 μL of nanozyme suspension (0.4 mg mL^{-1}) was first dropped onto diamond IRE, dried to form a sample film, and then 10 μL HCl solution (pH = 3.6) was added onto the sample film for background subtraction. Finally, 10 μL of H_2O_2 (1 mM) was dropped onto the film and the reaction began. At the same time, the spectra were also recorded using a liquid N$_2$-cooled mercury–cadmium–telluride detector.

2.7. Colorimetric sensing based on FeCo-MOF-H$_2$ nanozymes

**2.7.1. Detection of H_2O_2.** The detection of H_2O_2 was based on the increase in the absorbance of oxTMB at 652 nm; that is, FeCo-MOF-H$_2$ catalyzed the oxidation of colorless TMB to blue oxTMB. 8 μL of TMB (20 mM), 2 μL of H_2O_2 (100 mM), and 5 μL of FeCo-MOF-H$_2$ (1 mg mL^{-1}) were successively added into 185 μL of acetate buffer solution (0.2 M, pH = 3.6). After incubation for 15 min, the absorbance of the resulting solution at 652 nm was recorded with the multimode plate reader. Finally, the H_2O_2 concentration-dependent absorbance curve was obtained.

2.7.2. Detection of GSH. The detection of GSH was based on the attenuated absorbance of oxTMB. That is, the FeCo-MOF-H$_2$ nanozymes first catalyzed the oxidation of TMB to blue oxTMB in the presence of H_2O_2, and then the oxTMB was reduced to colorless TMB by GSH. Specifically, 8 μL of TMB (20 mM), 2 μL of H_2O_2 (100 mM), and 5 μL of FeCo-MOF-H$_2$ (1 mg mL^{-1}) were first added sequentially into 183 μL of acetate buffer solution (0.2 M, pH = 3.6). After chromogenic incubation for 10 min, 2 μL of different concentrations of GSH was added into the above solution for further attenuated reaction for 5 min. Then, the absorbances of the mixtures were measured. Finally, the GSH concentration-dependent attenuated absorbance ($\Delta A = A_{H_2O_2} - A_{GSH}$) curve was plotted.

3. Results and discussion

3.1. Synthesis and characterization of mixed-valence FeCo-MOF nanozymes

As shown in Fig. 1a, mixed-valence FeCo-MOF nanozymes (FeCo-MOF-H$_2$) were synthesized *via* a low-temperature heat treatment on Co doped MIL-53(Fe) under a H$_2$/Ar (5 : 95) atmosphere. In this process, low-temperature heat treatment was used to finely tune the electronic structure, chemical state, and coordination environment of Fe sites, and thus the appropriate temperature was a critical factor. To this end, TGA was first performed to determine the optimal heat treatment temperature (Fig. S1†). At 200 °C, adsorbed-water, solvent, and partial anion ligands (OH$^-$ and Cl$^-$) can be removed from the FeCo-MOF to form a large number of coordinatively unsaturated metal active sites for catalysis, while maintaining the original porous framework structure of MIL-53(Fe).[28] Therefore, heat treatment at 200 °C was chosen to adjust the coordination environment of metal nodes in the FeCo-MOF.
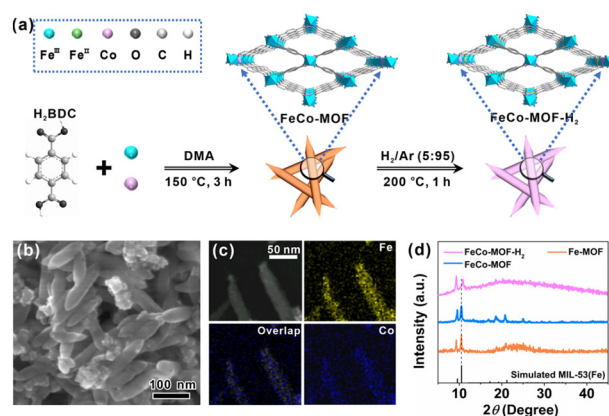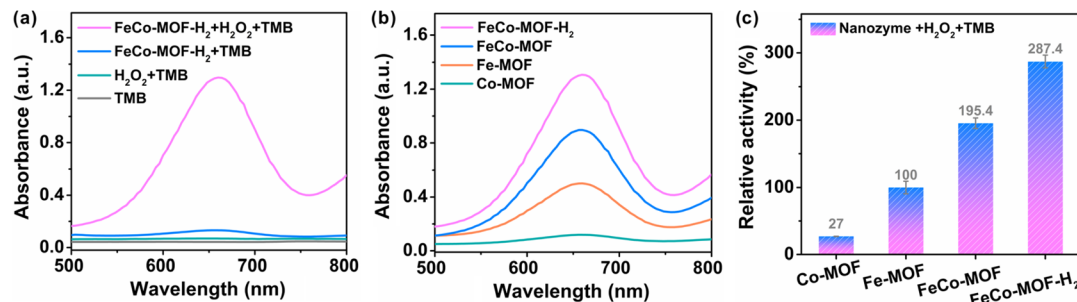

Fig. 1 (a) Schematic diagram of the synthesis of FeCo-MOF-H$_2$ nanozymes. (b) SEM image of FeCo-MOF-H$_2$. (c) HAADF-STEM image and corresponding EDS elemental mapping images of FeCo-MOF-H$_2$. (d) XRD patterns of the Fe-MOF, FeCo-MOF, and FeCo-MOF-H$_2$.

Fig. 1b shows an SEM image of the FeCo-MOF sample after heat treatment. It can be seen that the as-prepared FeCo-MOF-H$_2$ exhibited a shuttle-like nanorod morphology, which was the same as those for the Fe-MOF and FeCo-MOF (Fig. S2†). High-angle annular dark field scanning transmission electron microscopy (HAADF-STEM) coupled with EDS elemental mapping of FeCo-MOF-H$_2$ further confirmed the uniform distribution of Fe and Co elements in the shuttle-like nanorods (Fig. 1c). Powder XRD analysis and FT-IR spectroscopy were further performed to reveal the changes of the FeCo-MOF upon heat treatment under H$_2$/Ar. In Fig. 1d, it can be seen that the FeCo-MOF and FeCo-MOF-H$_2$ exhibited similar patterns to the Fe-MOF (MIL-53(Fe)), indicating that the doping of Co does not affect the crystal structure.[29] However, the peak at 10.5° exhibited a shift towards a higher angle in FeCo-MOF-H$_2$, which may be due to a slight change in unit cell parameters. Besides that, this characteristic peak broadened and decreased in intensity, implying a partial loss of long-range order following the formation of coordinatively unsaturated metal sites after heat treatment.[30] The semblable FT-IR spectra (Fig. S3†) further revealed that the metal–O$_{linker}$ peak in the FeCo-MOF and FeCo-MOF-H$_2$ shifted towards lower wavenumbers when compared to those of the Fe-MOF and Co-MOF, indicating the formation of bimetallic nodes of Fe and Co with different chemical environments.[31] The above results indicate the successful doping of Co ions into the Fe-MOF, and the framework structure is not damaged by heat treatment. Therefore, the fine construction of metal nodes in Fe-based MOF nanozymes can be tailored using this strategy.

3.2. Enzyme-mimicking activities of nanozymes

The enzyme-mimicking activities of FeCo-MOF-H$_2$ were evaluated by recording the absorbance of oxidized-TMB (oxTMB) at 652 nm. In Fig. 2a, an obvious absorption was observed with the coexistence of TMB, H_2O_2 and FeCo-MOF-H$_2$, whereas the absorption was negligible when the solution contained only

This journal is © the Partner Organisations 2023

Inorg. Chem. Front., 2023, **10**, 2335–2343 | **2337**

Fig. 2 (a) The absorption spectra of TMB, H_2O_2 + TMB, FeCo-MOF-H_2 + TMB, and FeCo-MOF-H_2 + H_2O_2 + TMB. (b) The absorption spectra of Co-MOF + H_2O_2 + TMB, Fe-MOF + H_2O_2 + TMB, FeCo-MOF + H_2O_2 + TMB, and FeCo-MOF-H_2 + H_2O_2 + TMB. (c) Comparison of peroxidase-like activities of Co-MOF, Fe-MOF, FeCo-MOF, and FeCo-MOF-H_2 nanozymes.

H_2O_2 or FeCo-MOF-H_2. This indicates that the FeCo-MOF-H_2 sample exhibited the peroxidase-like activity. As shown in Fig. S4,† the FeCo-MOF-H_2 nanozyme that was prepared *via* low-temperature heat treatment on the FeCo-MOF with 0.5 mmol of Fe and 1.8 mmol of Co salts showed the best peroxidase-like activity. Therefore, it was chosen as a mixed-valence FeCo-MOF nanozyme model for studying the structure–activity relationship. The peroxidase-like activities of control samples (Co-MOF, Fe-MOF, and FeCo-MOF) were also measured. As shown in Fig. 2b, the peroxidase-like activities of these samples were in the order of FeCo-MOF > Fe-MOF > Co-MOF, but they were much less active than FeCo-MOF-H_2. Interestingly, although the Co-MOF had a lower activity compared with the Fe-MOF, the catalytic activity of the Co-doped Fe-MOF (FeCo-MOF) was significantly higher than that of the former two single MOFs (Fig. 2c). The catalytic activity of this modulated FeCo-MOF-H_2 was about 10.6 and 2.9 times compared to those of pristine Co-MOF and Fe-MOF, respectively. All these results indicate that the peroxidase-like activity of these MOFs strongly depends on the fine structure of metal nodes, which controls the $^{\bullet}OH$ level generated by H_2O_2.

3.3. Synergistic recognition adsorption and catalytic mechanism study

Structurally, Fe^{III} sites in the pristine Fe-MOF are usually fully coordinated with terephthalic acid and other molecules or ions to form FeO_6 chains, which hinders the adsorption and decomposition of H_2O_2.[32] In this work, the incorporation of Co sites and low-temperature heat treatment were used to modulate the electronic structure, chemical state, and coordination environment of Fe sites (Fig. S5†). The high-resolution XPS spectra of Fe 2p, Co 2p and their directly adjacent O 1s in the metal–oxygen Fe–O–Co chain of FeCo-MOF-H_2 were systematically analyzed with the FeCo-MOF and Fe-MOF as references. As shown in Fig. 3a, due to the incorporation of Co sites, the peak of Fe $2p_{2/3}$ at 710 eV that was assigned to catalytically active Fe^{II} sites appeared in the FeCo-MOF, which is consistent with the reported literature.[33] Moreover, the content of Fe^{II} in FeCo-MOF-H_2 further increased (10.2% to 14.9%) after the low-temperature heat treatment under a H_2/Ar atmosphere, which was calculated from the proportion of the $Fe^{II}/(Fe^{II}$ +
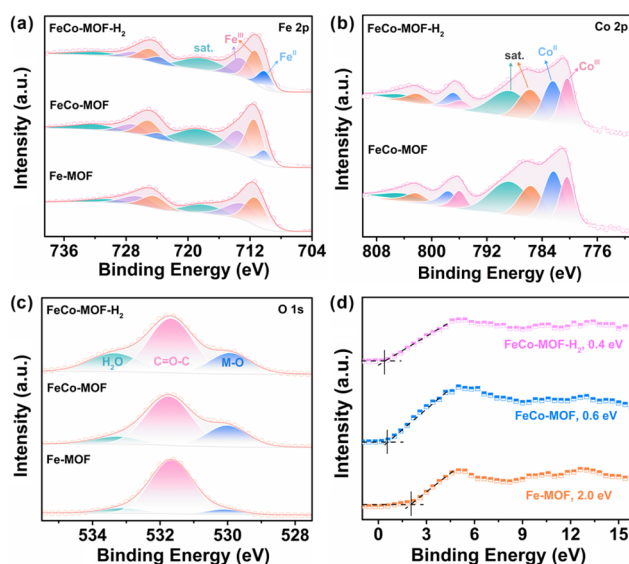
Fig. 3 (a) High-resolution Fe 2p XPS spectra of FeCo-MOF-H_2, FeCo-MOF and Fe-MOF. (b) High-resolution Co 2p XPS spectra of FeCo-MOF-H_2 and FeCo-MOF. (c) High-resolution O 1s XPS spectra of FeCo-MOF-H_2, FeCo-MOF and Fe-MOF. (d) Valence band structure of FeCo-MOF-H_2, FeCo-MOF and Fe-MOF.

Fe^{III} + sat.) XPS peak in Fe $2p_{3/2}$ as a reference. In Fig. 3b, the binding energy peak of Co $2p_{3/2}$ located at 781.1 eV can be deconvoluted into 780.4, 782.3, 785.6, and 788.7 eV, which are attributed to the Co^{II}, Co^{III} and their satellite-peaks, respectively.[34] With the addition of Co^{II} salt, the Co^{III} sites appeared in the FeCo-MOF, which may be due to the electron transfer from the Co^{II} to Fe^{III} sites through the Co–O–Fe bridging oxygen bond. Therefore, FeCo-MOF nanozymes had abundant mixed-valence metal sites of Fe^{II}, Fe^{III}, Co^{II} and Co^{III}. Moreover, the proportion of Co^{II} in FeCo-MOF-H_2 decreased slightly after low-temperature heat treatment under a H_2/Ar atmosphere. All the results indicate that the interfacial charge redistribution and the modulation of the coordination environment of Fe and Co sites construct abundant accessible catalytically active sites, which lead to easier H_2O_2 adsorption and catalytic decomposition.[35] In Fig. 3c, the high-resolution

spectrum of O 1s for FeCo-MOF-H_2 can be deconvoluted into three peaks located at 529.9 eV, 531.7 eV, and 533.4 eV, which can be ascribed to the Fe/Co–O band, O in the organic ligand, and adsorbed H_2O on defects created during synthesis, respectively.[36] It should be noted that the content of the Fe/Co–O band in these MOF nanozymes was very different. This indicates that the coordination status of metal sites in the FeCo-MOF and FeCo-MOF-H_2 significantly changed with the incorporation of Co sites and low-temperature heat treatment. Among the three Fe-based MOF samples, the content of adsorbed H_2O on the defects in FeCo-MOF-H_2 was the highest (21.95%). That is to say, FeCo-MOF-H_2 was more likely to enrich H_2O_2 to replace the adsorbed H_2O for peroxidase-like catalytic reaction, thereby exhibiting the highest peroxidase-like activity. In addition, the valence-band XPS spectra of nanozymes were investigated (Fig. 3d). The valence band maximum energy of the Fe-MOF was 2.0 eV, while the maximum valence band energies of the FeCo-MOF and FeCo-MOF-H_2 blue-shifted to the vacuum level at about 0.6 eV and 0.4 eV, respectively. Clearly, the changed electron structure due to Co-doping and low-temperature heat treatment was more conducive to electron transfer.[37] Therefore, the above results indicate that FeCo-MOF-H_2 has not only abundant and accessible catalytic metal sites, but also much lower electron transfer barriers. Owing to the synergistic adsorption and catalysis caused by its electronic and coordination architectures, FeCo-MOF-H_2 exhibited the best peroxidase-like catalytic activity.

In situ ATR-FTIR spectra were recorded to investigate the effect of the Co incorporation and low-temperature heat treatment on the adsorption process of nanozymes to the substrate H_2O_2 in the reaction (Fig. 4a–c). For the Fe-MOF, the absorption band at 1394 cm^{-1}, which is assigned to the OOH bending mode of adsorbed *H_2O_2 (HOOH$_{ad}$) onto the coordi-

natively unsaturated Fe sites of the Fe-MOF,[38] gradually increased with the reaction time (Fig. 4a). The absorption intensities of HOOH$_{ad}$ on the pristine Fe-MOF still remained unsaturated for 15 min, which indicates that the Fe sites in the Fe-MOF are almost completely coordinated and hinder the adsorption of H_2O_2. However, with the introduction of Co sites, the absorption intensities of HOOH$_{ad}$ for the FeCo-MOF rapidly reached saturation within only one minute (Fig. 4b). This suggests that the coordination environment or defect modulated by the incorporation of Co sites favors the FeCo-MOF to have more unsaturated coordination or available open sites for H_2O_2 adsorption than the Fe-MOF. This result is consistent with the inherent structural analysis of nanozymes in Fig. 3. Moreover, in Fig. 4c, the FeCo-MOF-H_2 also exhibited a similar phenomenon to the FeCo-MOF, showing that the low-temperature heat treatment did not affect the adsorption of H_2O_2 on FeCo-MOF-H_2 and no signals for the O–O stretching mode of physisorbed H_2O_2 at 880 cm^{-1} was observed, which suggests that H_2O_2 preferred to form surface complexes with Fe-based MOFs.[39] In addition, the O–O stretching mode of adsorbed O_2 was also not detected, indicating that the substrate of nanozymes is not O_2, or that the adsorbed oxygen molecules were very little.[38] As a result, the oxidase-like catalytic activity of these samples can be negligible, which is consistent with the result in Fig. 2. ESR was further conducted with DMPO as a specific radical probe to reveal the intermediate generated from HOOH$_{ad}$ catalyzed by FeCo-MOF-H_2. As shown in Fig. 4d, the mixture of H_2O_2 and FeCo-MOF-H_2 exhibited a characteristic 1:2:2:1 quadruple signal of DMPO-$^{\bullet}$OH, indicating that the FeCo-MOF-H_2 can catalyze the decomposition of HOOH$_{ad}$ into $^{\bullet}$OH.[27]

Based on the above results, the peroxidase-like catalytic process over FeCo-MOF-H_2 is depicted in the schematic diagram in Fig. 4e. (1) Substrate H_2O_2 diffusion transport and selective adsorption process: due to the incorporation of Co and low-temperature thermal treatment, FeCo-MOF-H_2 possesses a large number of accessible active sites, such as Fe^{II}–O–Fe/Co sites. Free H_2O_2 in the bulk solution first diffuses to the accessible open Fe^{II}–O–Fe/Co sites in FeCo-MOF-H_2, and the selective adsorption reaches saturation rapidly, forming surface complexes with the MOF (HOOH$_{ad}$). (2) The HOOH$_{ad}$ catalytic process over Fe^{II} or Co^{II} sites: typically, the O–O bond of HOOH$_{ad}$ is cleaved after accepting electrons from Fe^{II}-O–Fe/Co, and dissociated into $^{\bullet}$OH. At the same time, Fe^{II}–O–Fe/Co is transformed into Fe^{III}–O–Fe/Co. (3) Oxidation process of TMB: the produced $^{\bullet}$OH oxidizes TMB to blue oxTMB. At the same time, Fe^{III}–O–Fe/Co in FeCo-MOF-H_2 is reduced to Fe^{II}–O–Fe/Co by H_2O_2, thus returning to its original state. It should be pointed out that the incorporated Co-sites not only increase the adsorption of H_2O_2 at accessible open sites and Fe^{II} catalytically active sites, but also catalyze the decomposition of H_2O_2. Although the catalytic activity of Co is weaker than that of Fe, Fe sites can accelerate the formation of Co catalytic sites according to the standard redox potential.[40] In short, the superior peroxidase-like performance of FeCo-MOF-H_2 is achieved by the selective and rapid saturation adsorption of
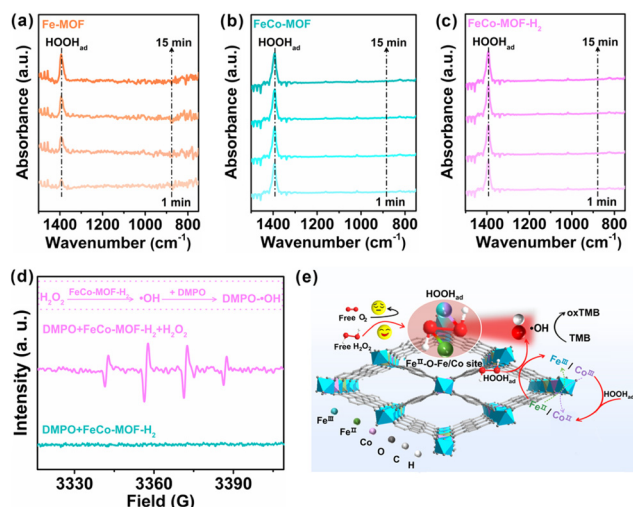
Fig. 4 *In situ* ATR-FTIR spectra of H_2O_2 adsorption on (a) Fe-MOF, (b) FeCo-MOF, and (c) FeCo-MOF-H_2 nanozymes in pH = 3.6 HCl solution. (d) The ESR spectra of DMPO + FeCo-MOF-H_2 and DMPO + FeCo-MOF-H_2 + H_2O_2. (e) The schematic diagram of the peroxidase-like catalytic mechanism of FeCo-MOF-H_2 nanozymes.

This journal is © the Partner Organisations 2023

Inorg. Chem. Front., 2023, **10**, 2335–2343 | **2339**

the substrate H_2O_2 and the synergistic catalysis of multiple metal sites.

3.4. Steady-state kinetic studies of nanozymes

To further evaluate the catalytic kinetics of FeCo-MOF-H_2 nanozymes, the steady-state kinetic assays were performed by varying one of the concentrations of H_2O_2 and TMB while maintaining the other. Fig. 5a and b show the Michaelis–Menten curves of FeCo-MOF-H_2 nanozymes against H_2O_2 and TMB, respectively. The double-reciprocal plots of FeCo-MOF-H_2 in Fig. 5c were calculated from the Michaelis–Menten curves. The kinetics constants including the Michaelis–Menten constant (K_m) and maximum reaction rate (ν_{max}) were calculated from the double-reciprocal plot according to the following equation:

$$\frac{1}{\nu} = \frac{K_m}{\nu_{max}} \times \frac{1}{[S]} + \frac{1}{\nu_{max}}$$

where ν and $[S]$ are the initial velocity and substrate concentration, respectively.

K_m refers to the affinity of nanozymes to the substrate, while ν_{max} implies the enzyme-mimicking activity. Fig. 5d shows the K_m and ν_{max} for FeCo-MOF-H_2 toward H_2O_2 and TMB, wherein the K_m value of FeCo-MOF-H_2 towards H_2O_2 was only 0.06 mM, significantly lower than that of TMB. Strikingly, FeCo-MOF-H_2 exhibited a higher affinity to H_2O_2 even when compared with natural HRP as well as reported Fe-based and Co-based nanozymes (Table 1).[41–51] Furthermore, FeCo-MOF-H_2 has a larger ν_{max} than most of those nanozymes. These results also confirmed that the multiple sites of Co and Fe^{II} contribute to the synergistic adsorption and catalysis on MOF-based nanozymes. As a result, the as-synthesized FeCo-

Table 1 The kinetic constants of other related Fe-based or Co-based nanozymes with H_2O_2 as the substrate

| Nanozymes	K_m [mM]	ν_{max} [M s^{-1}]	Ref.
Fe-MOF	0.15	9.2×10^{-9}	41
Fe-MIL-88NH$_2$	2.06	7.04×10^{-8}	42
2D Co-MOF	0.24	5.01×10^{-7}	43
Co/Fe-MOFs	5.37	2.71×10^{-8}	44
MIL-101(Co,Fe)@MIP	2.325	—	45
MOF-919 (Fe–Cu)	1.36	1.462×10^{-7}	46
Fe$_3$O$_4$	154	9.78×10^{-8}	47
Co$_3$O$_4$	5.9322	9.85×10^{-8}	48
Fe SACs	0.243	8.25×10^{-8}	49
SA Co-MoS$_2$	3.349	6.49×10^{-7}	50
HRP	3.7	8.71×10^{-8}	51
FeCo-MOF-H$_2$	0.06	1.6×10^{-7}	This work

MOF-H_2 can increase the utilization of H_2O_2 and fully decompose it into $^{\bullet}OH$, thereby having great potential in improving the detection limit of H_2O_2 and performance of biomedical therapy.
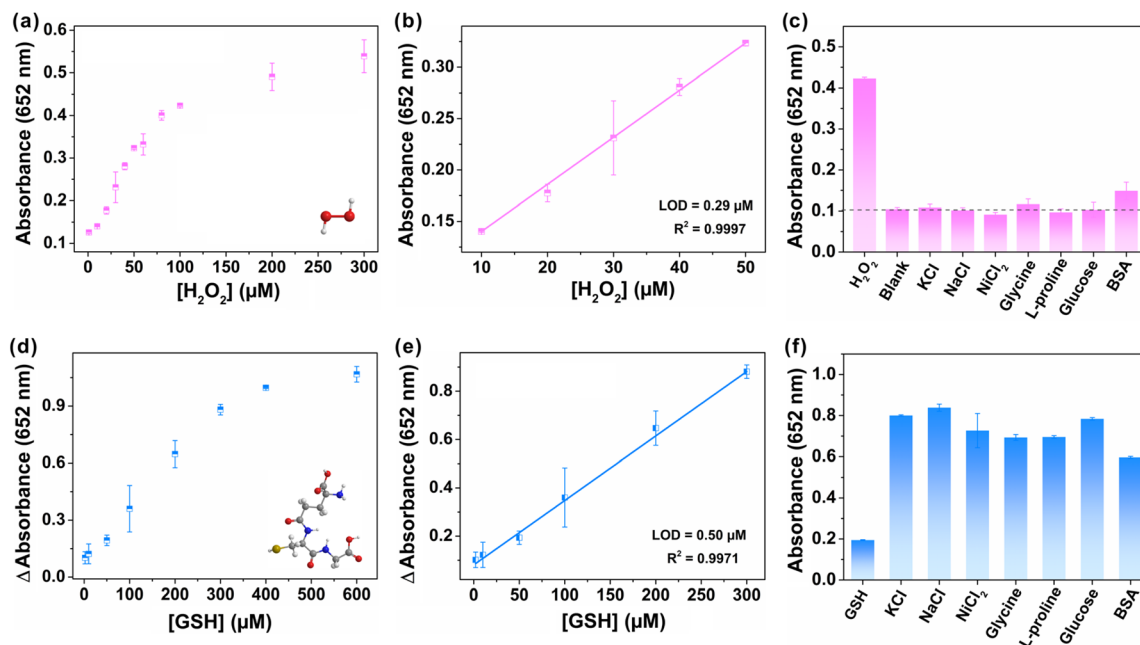
3.5. Sensing application of FeCo-MOF-H_2 acting as peroxidase-like nanozymes

As a proof-of-concept application, FeCo-MOF-H_2 were first applied to sensitive detection of H_2O_2 that is closely associated with a variety of diseases.[27] As shown in Fig. 6a, the absorbance of produced oxTMB increased with the successive addition of H_2O_2. The FeCo-MOF-H_2 nanozyme based sensor demonstrated a good linear relationship in the range of 10–50 μM with a limit of detection (LOD) of 0.29 μM (Fig. 6b). In fact, the LOD of FeCo-MOF-H_2 was only worse than that of Fe based single atom catalysts, but far better than those of other reported Fe-based or Co-based nanozymes (Table S1†). In addition, a variety of potentially interfering substrates at five-fold higher concentrations than H_2O_2 were investigated for selective assays for the detection of H_2O_2, including KCl, NaCl, NiCl$_2$, glycine, L-proline, glucose and BSA (bovine serum albumin), and the results are summarized in Fig. 6c. Signals from most of these interfering substrates were negligible, except for a slight absorbance of BSA. This phenomenon is consistent with the report that BSA can enhance the enzymatic activity, indicating that the FeCo-MOF-H_2 nanozymes fully conform to the characteristics of natural enzymes.[52] Therefore, the high affinity and catalytic activity of FeCo-MOF-H_2 towards to H_2O_2 contributed to a low LOD, which allows sensitive monitoring of weak fluctuation for H_2O_2.

In addition to detecting color-enhancing target molecules, the FeCo-MOF-H_2 nanozymes were also used to detect the reductive biothiol molecule GSH, which further reduced blue oxTMB to colorless TMB with the attenuation of oxTMB absorbance at 652 nm. As shown in Fig. 6d, the attenuated absorbance of the reaction solution at 652 nm increased with increasing GSH concentration. In Fig. 6e, the fitting curve derived from Fig. 6d exhibited a good linear relationship in a wide GSH concentration range from 2 μM to 300 μM, which was significantly wider than those of other nanozymes in
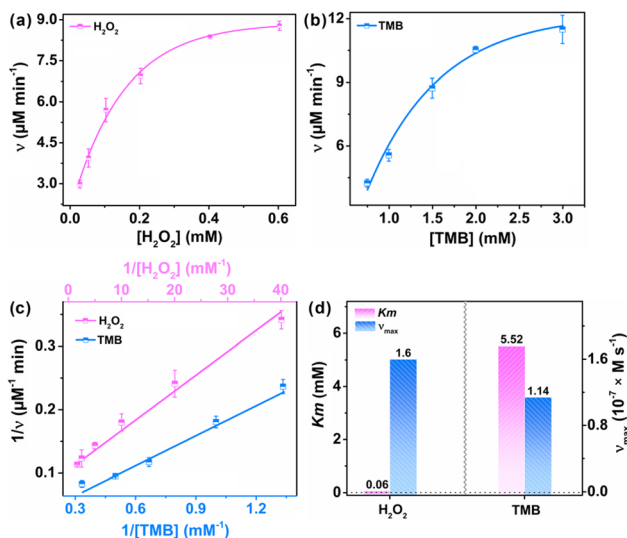
Fig. 5 Steady-state kinetic assay of FeCo-MOF-H_2 nanozymes. The Michaelis–Menten curves of FeCo-MOF-H_2 nanozymes toward (a) H_2O_2 and (b) TMB. (c) The corresponding double-reciprocal plots of FeCo-MOF-H_2 nanozymes. (d) Histograms of K_m and ν_{max} for FeCo-MOF-H_2 nanozymes toward H_2O_2 and TMB.

2340 | *Inorg. Chem. Front.*, 2023, **10**, 2335–2343

This journal is © the Partner Organisations 2023

Fig. 6 (a) Relationship between increased absorbance and H_2O_2 concentration. (b) Linear range for colorimetric detection of H_2O_2. (c) Selectivity test for detecting H_2O_2. (d) Relationship between attenuated absorbance and GSH concentration. (e) Linear range for colorimetric detection of GSH. (f) Selectivity test for detecting GSH.

Table S2.† This result indicated that the high peroxidase-like catalytic activity of FeCo-MOF-H_2 can contribute to the wide linear detection range of reduced GSH, which is close to the true concentration of intracellular GSH.[53] In addition, FeCo-MOF-H_2 had a LOD of 0.50 μM, which is comparable to those of other reported Fe-based or Co-based nanozymes. In Fig. 6f, although the concentrations of potential interferents were 5-fold higher than those of GSH, the observed absorbance changes in the presence of GSH were significantly lower than those of the potential substrates. The results indicated that the FeCo-MOF-H_2 based colorimetric sensor towards GSH detection possessed satisfactory selectivity.

4. Conclusions

In this study, mixed-valence FeCo-MOF nanozymes were designedly prepared by low-temperature heat treatment using FeCo-MOF as the precursor. Different from previous studies, the recognition adsorption and catalytic mechanisms of the as-synthesized FeCo-MOF-H_2 nanozymes were systematically studied by a variety of spectroscopic methods. We found that the as-prepared FeCo-MOF-H_2 exhibited significantly enhanced specific peroxidase-like activity, which was ascribed to the synergistic adsorption and catalysis of abundant accessible metal sites. Notably, FeCo-MOF-H_2 peroxidase-like nanozymes exhibited high affinity and catalytic activity compared with most reported HRP and Fe/Co-based nanozymes, thereby showing excellent selectivity and sensitivity in detecting H_2O_2 and GSH. This study well highlights the synergistic adsorption

and catalysis of mixed-metal nodes in MOF-based nanozymes, and provides a meaningful reference to rationally design nanozymes with high selectivity and catalytic activity.

Conflicts of interest

There are no conflicts to declare.

Acknowledgements

References

1 J. Wu, X. Wang, Q. Wang, Z. Lou, S. Li, Y. Zhu, L. Qin and H. Wei, Nanomaterials with enzyme-like characteristics (nanozymes): next-generation artificial enzymes (II), *Chem. Soc. Rev.*, 2019, **48**, 1004–1076.

2 H. Wei, L. Gao, K. Fan, J. Liu, J. He, X. Qu, S. Dong, E. Wang and X. Yan, Nanozymes: A clear definition with fuzzy edges, *Nano Today*, 2021, **40**, 101269.

3 Z. Wang, R. Zhang, X. Yan and K. Fan, Structure and activity of nanozymes: Inspirations for de novo design of nanozymes, *Mater. Today*, 2020, **41**, 81–119.

4 O. Adeniyi, S. Sicwetsha and P. Mashazi, Nanomagnet-silica nanoparticles decorated with Au@Pd for enhanced

This journal is © the Partner Organisations 2023

Inorg. Chem. Front., 2023, **10**, 2335–2343 | **2341**

peroxidase-like activity and colorimetric glucose sensing, *ACS Appl. Mater. Interfaces*, 2020, **12**, 1973–1987.

5 M. Zhao, H. B. Wang, L. N. Ji and Z. W. Mao, Insights into metalloenzyme microenvironments: biomimetic metal complexes with a functional second coordination sphere, *Chem. Soc. Rev.*, 2013, **42**, 8360–8375.

6 M. S. Kim, J. Lee, H. S. Kim, A. Cho, K. H. Shim, T. N. Le, S. S. A. An, J. W. Han, M. I. Kim and J. Lee, Heme cofactor-resembling Fe–N single site embedded graphene as nanozymes to selectively detect H_2O_2 with high sensitivity, *Adv. Funct. Mater.*, 2020, **30**, 1905410.

7 W. Xu, Y. Kang, L. Jiao, Y. Wu, H. Yan, J. Li, W. Gu, W. Song and C. Zhu, Tuning atomically dispersed Fe sites in metal–organic frameworks boosts peroxidase-like activity for sensitive biosensing, *Nano-Micro Lett.*, 2020, **12**, 184.

8 R. Zhang, X. Yan and K. Fan, Nanozymes inspired by natural enzymes, *Acc. Mater. Res.*, 2021, **2**, 534–547.

9 Z. Xi, K. Wei, Q. Wang, M. J. Kim, S. Sun, V. Fung and X. Xia, Nickel-platinum nanoparticles as peroxidase mimics with a record high catalytic efficiency, *J. Am. Chem. Soc.*, 2021, **143**, 2660–2664.

10 Y. Wang, G. Jia, X. Cui, X. Zhao, Q. Zhang, L. Gu, L. Zheng, L. H. Li, Q. Wu, D. J. Singh, D. Matsumura, T. Tsuji, Y.-T. Cui, J. Zhao and W. Zheng, Coordination number regulation of molybdenum single-atom nanozyme peroxidase-like specificity, *Chem*, 2021, **7**, 436–449.

11 L. Zhang, Z. Liu, Q. Deng, Y. Sang, K. Dong, J. Ren and X. Qu, Nature-inspired construction of MOF@COF nanozyme with active sites in tailored microenvironment and pseudopodia-like surface for enhanced bacterial inhibition, *Angew. Chem., Int. Ed.*, 2021, **60**, 3469–3474.

12 S. Ji, B. Jiang, H. Hao, Y. Chen, J. Dong, Y. Mao, Z. Zhang, R. Gao, W. Chen, R. Zhang, Q. Liang, H. Li, S. Liu, Y. Wang, Q. Zhang, L. Gu, D. Duan, M. Liang, D. Wang, X. Yan and Y. Li, Matching the kinetics of natural enzymes with a single-atom iron nanozyme, *Nat. Catal.*, 2021, **4**, 407–417.

13 J. Wu, Z. Wang, X. Jin, S. Zhang, T. Li, Y. Zhang, H. Xing, Y. Yu, H. Zhang, X. Gao and H. Wei, Hammett relationship in oxidase-mimicking metal-organic frameworks revealed through a protein-engineering-inspired strategy, *Adv. Mater.*, 2021, **33**, 2005024.

14 Z. Wang, B. Liu, Q. Sun, L. Feng, F. He, P. Yang, S. Gai, Z. Quan and J. Lin, Upconverted metal-organic framework Janus architecture for near-infrared and ultrasound Co-enhanced high performance tumor therapy, *ACS Nano*, 2021, **15**, 12342–12357.

15 M. Li, J. Chen, W. Wu, Y. Fang and S. Dong, Oxidase-like MOF-818 nanozyme with high specificity for catalysis of catechol oxidation, *J. Am. Chem. Soc.*, 2020, **142**, 15569–15574.

16 X. Zhang, X. Huang, Z. Wang, Y. Zhang, X. Huang, Z. Li, M. Daglia, J. Xiao, J. Shi and X. Zou, Bioinspired nanozyme enabling glucometer readout for portable monitoring of pesticide under resource-scarce environments, *Chem. Eng. J.*, 2022, **429**, 132243.

17 I. Nath, J. Chakraborty and F. Verpoort, Metal organic frameworks mimicking natural enzymes: a structural and functional analogy, *Chem. Soc. Rev.*, 2016, **45**, 4127–4170.

18 K. Chen and C.-D. Wu, Designed fabrication of biomimetic metal-organic frameworks for catalytic applications, *Coord. Chem. Rev.*, 2019, **378**, 445–465.

19 P. Yang, J. Tao, F. Chen, Y. Chen, J. He, K. Shen, P. Zhao and Y. Li, Multienzyme-mimic ultrafine alloyed nanoparticles in metal organic frameworks for enhanced chemodynamic therapy, *Small*, 2021, **17**, 2005865.

20 R. A. Fischer, Z. Zhou, S. Mukherjee, S. Hou, W. Li and M. Elsner, Porphyrinic MOF film for multifaceted electrochemical sensing, *Angew. Chem., Int. Ed.*, 2021, **60**, 20551–20557.

21 Y. Zhang, Y. S. Feng, X. H. Ren, X. W. He, W. Y. Li and Y. K. Zhang, Bimetallic molecularly imprinted nanozyme: Dual-mode detection platform, *Biosens. Bioelectron.*, 2022, **196**, 113718.

22 Q. Zhou, H. Yang, X. Chen, Y. Xu, D. Han, S. Zhou, S. Liu, Y. Shen and Y. Zhang, Cascaded nanozyme system with high reaction selectivity by substrate screening and channeling in a microfluidic device, *Angew. Chem., Int. Ed.*, 2022, **61**, 202112453.

23 Q. Chen, Y. Liu, Y. Lu, Y. Hou, X. Zhang, W. Shi and Y. Huang, Atomically dispersed Fe/Bi dual active sites single-atom nanozymes for cascade catalysis and peroxymonosulfate activation to degrade dyes, *J. Hazard. Mater.*, 2022, **422**, 126929.

24 C. B. Ma, Y. Xu, L. Wu, Q. Wang, J. J. Zheng, G. Ren, X. Wang, X. Gao, M. Zhou, M. Wang and H. Wei, Guided synthesis of a Mo/Zn dual single-atom nanozyme with synergistic effect and peroxidase-like activity, *Angew. Chem., Int. Ed.*, 2022, **61**, 2021161.

25 X. Li, P. Liu, X. Niu, K. Ye, L. Ni, D. Du, J. Pan and Y. Lin, Tri-functional Fe-Zr bi-metal–organic frameworks enable high-performance phosphate ion ratiometric fluorescent detection, *Nanoscale*, 2020, **12**, 19383–19389.

26 L. Luo, Y. Ou, Y. Yang, G. Liu, Q. Liang, X. Ai, S. Yang, Y. Nian, L. Su and J. Wang, Rational construction of a robust metal-organic framework nanozyme with dual-metal active sites for colorimetric detection of organophosphorus pesticides, *J. Hazard. Mater.*, 2022, **423**, 127253.

27 X. Cheng, X. Zhou, Z. Zheng and Q. Kuang, Construct efficient substrate transport and catalytic sub-nanochannels in metal-organic framework-based nanozymes for boosting peroxidase-like catalytic activity, *Chem. Eng. J.*, 2022, **430**, 133079.

28 H. Liang, R. Liu, X. An, C. Hu, X. Zhang and H. Liu, Bimetal-organic frameworks with coordinatively unsaturated metal sites for highly efficient Fenton-like catalysis, *Chem. Eng. J.*, 2021, **414**, 128669.

29 P. L. Llewellyn, P. Horcajada, G. Maurin, T. Devic, N. Rosenbach, S. Bourrelly, C. Serre, D. Vincent, S. Loera-Serna, Y. Filinchuk and G. Férey, Complex adsorption of short linear alkanes in the flexible metal-organic-framework MIL-53 (Fe), *J. Am. Chem. Soc.*, 2009, **131**, 13002–13008.

2342 | *Inorg. Chem. Front.*, 2023, **10**, 2335–2343

This journal is © the Partner Organisations 2023

30 S. Peng, R. Li, Y. Rao, Y. Huang, Y. Zhao, M. Xiong, J. Cao and S. Lee, Tuning the unsaturated iron sites in MIL-101(Fe) nanoparticles for reactive oxygen species-mediated bacterial inactivation in the dark, *Appl. Catal., B*, 2022, **316**, 121693.

31 Z. Wang, C. Wu, Z. Zhang, Y. Chen, W. Deng and W. Chen, Bimetallic Fe/Co-MOFs for tetracycline elimination, *J. Mater. Sci.*, 2021, **56**, 15684–15697.

32 L. Tao, C. Lin, S. Dou, S. Feng, D. Chen, D. Liu, J. Huo, Z. Xia and S. Wang, Creating coordinatively unsaturated metal sites in metal-organic-frameworks as efficient electrocatalysts for the oxygen evolution reaction: Insights into the active centers, *Nano Energy*, 2017, **41**, 417–425.

33 S. Lv, J. Liu, N. Zhao, C. Li, Z. Wang and S. Wang, A novel cobalt doped MOF-based photocatalyst with great applicability as an efficient mediator of peroxydisulfate activation for enhanced degradation of organic pollutants, *New J. Chem.*, 2020, **44**, 1245.

34 D. Liu, M. Li, X. Li, F. Ren, P. Sun and L. Zhou, Core-shell Zn/Co MOFs derived Co_3O_4/CNTs as an efficient magnetic heterogeneous catalyst for persulfate activation and oxytetracycline degradation, *Chem. Eng. J.*, 2020, **387**, 124008.

35 M. Giménez-Marqués, A. Santiago-Portillo, S. Navalón, M. Álvaro, V. Briois, F. Nouar, H. Garcia and C. Serre, Exploring the catalytic performance of a series of bimetallic MIL-100(Fe, Ni) MOFs, *J. Mater. Chem. A*, 2019, **7**, 20285–20292.

36 Z. Zhao, D. Yang, H. Ren, K. An, Y. Chen, Z. Zhou, W. Wang and Z. Jiang, Nitrogenase-inspired mixed-valence MIL-53 (Fe^{II}/Fe^{III}) for photocatalytic nitrogen fixation, *Chem. Eng. J.*, 2020, **400**, 125929.

37 Z. Xue, Y. Li, Y. Zhang, W. Geng, B. Jia, J. Tang, S. Bao, H.-P. Wang, Y. Fan, Z.-w. Wei, Z. Zhang, Z. Ke, G. Li and C.-Y. Su, Modulating electronic structure of metal-organic framework for efficient electrocatalytic oxygen evolution, *Adv. Energy Mater.*, 2018, **8**, 1801564.

38 C. Tang, L. Chen, H. Li, L. Li, Y. Jiao, Y. Zheng, H. Xu, K. Davey and S. Z. Qiao, Tailoring acidic oxygen reduction selectivity on single-atom catalysts via modification of first and second coordination spheres, *J. Am. Chem. Soc.*, 2021, **143**, 7819–7827.

39 W. Y. Lin and H. Frei, Photochemical and FT-IR probing of the active site of hydrogen peroxide in Ti silicalite sieve, *J. Am. Chem. Soc.*, 2002, **124**, 9292–9298.

40 Z. Zhu, C. Ji, L. Zhong, S. Liu, F. Cui, H. Sun and W. Wang, Magnetic Fe–Co crystal doped hierarchical porous carbon fibers for removal of organic pollutants, *J. Mater. Chem. A*, 2017, **5**, 18071–18080.

41 D. Hou, Y. You, X. Wu, C. Li, S. Wu, C. Zhang and Y. Xian, A nanosized metal–organic framework for visual detection of fluoride ions with smartphone via colorimetric test kit, *Sens. Actuators, B*, 2021, **332**, 129508.

42 Y. L. Liu, X. J. Zhao, X. X. Yang and Y. F. Li, A nanosized metal–organic framework of Fe-MIL-88NH$_2$ as a novel peroxidase mimic used for colorimetric detection of glucose, *Analyst*, 2013, **138**, 4526–4531.

43 H. Wan, Y. Wang, J. Chen, H. M. Meng and Z. Li, 2D Co-MOF nanosheet-based nanozyme with ultrahigh peroxidase catalytic activity for detection of biomolecules in human serum samples, *Microchim. Acta*, 2021, **188**, 130.

44 X. L. Zhao, J. L. Liu, F. T. Xie, T. Yang, R. Hu and Y. H. Yang, Iodide-enhanced Co/Fe-MOFs nanozyme for sensitively colorimetric detection of H_2S, *Spectrochim. Acta, Part A*, 2021, **262**, 120117.

45 Y. Zhang, Y. S. Feng, X. H. Ren, X. W. He, W. Y. Li and Y. K. Zhang, Bimetallic molecularly imprinted nanozyme: Dual-mode detection platform, *Biosens. Bioelectron.*, 2022, **196**, 113718.

46 S. Kulandaivel, C. H. Lin and Y. C. Yeh, The bi-metallic MOF-919 (Fe-Cu) nanozyme capable of bifunctional enzyme-mimicking catalytic activity, *Chem. Commun.*, 2022, **58**, 569–572.

47 L. Gao, J. Zhuang, L. Nie, J. Zhang, Y. Zhang, N. Gu, T. Wang, J. Feng, D. Yang, S. Perrett and X. Yan, Intrinsic peroxidase-like activity of ferromagnetic nanoparticles, *Nat. Nanotechnol.*, 2007, **2**, 577–583.

48 X. Liu, L. Yan, H. Ren, Y. Cai, C. Liu, L. Zeng, J. Guo and A. Liu, Facile synthesis of magnetic hierarchical flower-like Co_3O_4 spheres: Mechanism, excellent tetra-enzyme mimics and their colorimetric biosensing applications, *Biosens. Bioelectron.*, 2020, **165**, 112342.

49 C. Zhao, C. Xiong, X. Liu, M. Qiao, Z. Li, T. Yuan, J. Wang, Y. Qu, X. Wang, F. Zhou, Q. Xu, S. Wang, M. Chen, W. Wang, Y. Li, T. Yao, Y. Wu and Y. Li, Unraveling the enzyme-like activity of heterogeneous single atom catalyst, *Chem. Commun.*, 2019, **55**, 2285–2288.

50 Y. Wang, K. Qi, S. Yu, G. Jia, Z. Cheng, L. Zheng, Q. Wu, Q. Bao, Q. Wang, J. Zhao, X. Cui and W. Zheng, Revealing the Intrinsic Peroxidase-Like Catalytic Mechanism of Heterogeneous Single-Atom Co-MoS$_2$, *Nano-Micro Lett.*, 2019, **11**, 102.

51 X. Ruan, D. Liu, X. Niu, Y. Wang, C. D. Simpson, N. Cheng, D. Du and Y. Lin, 2D Graphene oxide/Fe-MOF nanozyme nest with superior peroxidase-like activity and its application for detection of woodsmoke exposure biomarker, *Anal. Chem.*, 2019, **91**, 13847–13854.

52 C. Riccardi, S. McCormick, R. Kasi and C. Kumar, A modular approach for interlocking enzymes in whatman paper, *Angew. Chem., Int. Ed.*, 2018, **57**, 10158–10162.

53 X. Huang, F. Xia and Z. Nan, Fabrication of FeS_2/SiO_2 double mesoporous hollow spheres as an artificial peroxidase and rapid determination of H_2O_2 and glutathione, *ACS Appl. Mater. Interfaces*, 2020, **12**, 46539–46548.

This journal is © the Partner Organisations 2023

Inorg. Chem. Front., 2023, **10**, 2335–2343 | **2343**